

Full Paper

Single-phase and multiphase models for temperature and relative humidity calculations during forced convection in a rubber-sheet drying chamber

Racha Dejchanchaiwong^{1, 2}, Yutthana Tirawanichakul^{1, 3}, Supawan Tirawanichakul^{1, 2} and Perapong Tekasakul^{1, 4, *}

¹ Energy Technology Research Centre (ETRC), Faculty of Engineering, Prince of Songkla University, Hat Yai, Songkhla 90112, Thailand

² Department of Chemical Engineering, Faculty of Engineering, Prince of Songkla University, Hat Yai, Songkhla 90112, Thailand

³ Department of Physics, Faculty of Science, Prince of Songkla University, Hat Yai, Songkhla 90112, Thailand

⁴ Department of Mechanical Engineering, Faculty of Engineering, Prince of Songkla University, Hat Yai, Songkhla 90112, Thailand

*Corresponding author, e-mail: perapong.t@psu.ac.th

Received: 29 August 2013 / Accepted: 4 August 2014 / Published: 25 August 2014

Abstract: Computational fluid dynamics modelling of single-phase and multiphase flows was used to simulate the temperature and relative humidity at various locations in an empty rubber-sheet drying chamber. In all planes, unlike the single-phase model, the multiphase model's temperature distribution is relatively uniform, and the temperature deviations are 0.01-4.73°C in the bottom plane, 0.02-4.05°C in the middle plane, and 0.01-3.84°C in the top plane. The single-phase model results in temperature deviations of 0.55-6.63°C, 0.02-6.02°C and 0.36-3.89°C in the bottom, middle and top planes respectively. Thus, the multiphase model is deemed superior. The inclusion of water vapour in the multiphase model increases the agreement between model and experimental temperature data. The largest temperature deviations occur at the centre-frontal positions of all planes owing to the turbulence of the hot gas at the inlet. In all planes the relative humidity is almost uniform, except near the centre-frontal area of the bottom plane. Clearly, the multiphase model is more appropriate for simulating chambers containing rubber sheets, though the diffusion of moisture from rubber sheets needs to be considered as well.

Keywords: natural rubber, rubber-sheet drying, multiphase model

INTRODUCTION

Multiphase flow is the simultaneous flow of fluids at different states or with different phases. Multiphase models have been widely used in engineering applications. However, to date, most numerical simulations and physical modelling are based on single-phase methods. Nonetheless, computational modelling of multiphase flow has been used to study complex multi-component systems. The use of computational fluid dynamics (CFD) is increasingly becoming popular in modelling fluid flow and heat and mass transfer because CFD is an accurate, effective and cost-efficient method [1-5]. Simultaneous heat and mass transfer under transient conditions is common in drying processes and CFD simulations have been widely used to analyse problems of fluid flow in drying processes [6-12]. Understanding fluid flow and heat transfer in the natural-rubber smoking process will help improve rubber's drying process and quality. Several previous studies have reported the use of the CFD modelling of single-phase fluid flow and heat transfer in rubber-smoking rooms [13, 14]. In this study, we used CFD simulation of single-phase and multiphase models to obtain the temperature and relative humidity in an empty rubber-sheet drying chamber and to assess the effect of a second phase (vapour).

SIMULATION APPROACH

Velocity, temperature and moisture can be determined by solving the continuity, momentum and energy equations respectively for fluid flow and heat and mass transfer, along with appropriate boundary conditions.

Governing Equations

Fluid flow can be described by the governing partial differential equations of mass, momentum and energy. Results are determined by solving these equations simultaneously. The governing equations for incompressible flow and Newtonian fluid are given by the following [15]:

Continuity equation

$$\frac{\partial \rho}{\partial t} + \nabla \cdot (\rho \bar{\mathbf{u}}) = 0 \quad (1)$$

Momentum equation

$$\frac{\partial (\rho \bar{\mathbf{u}})}{\partial t} + \nabla \cdot (\rho \bar{\mathbf{u}} \bar{\mathbf{u}}) = -\nabla P + \nabla \cdot \left[\mu_{eff} (\nabla \bar{\mathbf{u}} + \nabla \bar{\mathbf{u}}^T) - \frac{2}{3} \nabla \cdot \bar{\mathbf{u}} \bar{\mathbf{I}} \right] - \rho g \beta (\bar{T} - \bar{T}_o) \quad (2)$$

Energy equation

$$\frac{\partial (\rho E)}{\partial t} + \nabla \cdot (\bar{\mathbf{u}} (\rho E + P)) = \nabla \cdot \left(\lambda_{eff} \nabla \bar{T} - \sum_j H_j \mathbf{J}_j + (\bar{\mathbf{t}}_{eff} \cdot \bar{\mathbf{u}}) \right) + S_E \quad (3)$$

where $\bar{\mathbf{u}}$ is the vector velocity (m/s), P is the pressure (N/m²), ρ is the density (kg/m³), g is the gravitational acceleration vector (m/s²), β is the thermal expansion coefficient, μ_{eff} is the effective viscosity (kg/m s), $\bar{\mathbf{u}}^T$ is the transposed mean velocity (m/s), \bar{T}_o is the system surrounding temperature (reference temperature, K), \bar{T} is the temperature (K), $\bar{\mathbf{I}}$ is the unit tensor, λ_{eff} is the effective conductivity (W/m K), t is the time (s), \mathbf{J}_j is the diffusion flux of species j (kg/m²s),

H_j is the enthalpy of species j (J/kg), $\bar{\tau}_{eff}$ is the effective stress tensor, S_E is the source term, and E is the total energy:

$$E = H - \frac{P}{\rho} + \frac{u^2}{2} \quad (4)$$

where H is the enthalpy (J/kg), u is the velocity (m/s), and $\frac{u^2}{2}$ represents the kinetic energy.

For turbulent flow, Reynolds stress and turbulent heat flux can be calculated using the standard $k-\varepsilon$ model [13]. The equations for the kinetic energy of turbulence (k in the $k-\varepsilon$ model) and its dissipation rate (ε) are the following [15, 16]:

k Equation

$$\frac{\partial(\rho k)}{\partial t} + \frac{\partial(\rho \bar{\mathbf{u}}_i k)}{\partial x_i} = \frac{\partial}{\partial x_i} \left[\left(\mu + \frac{\mu_t}{\sigma_k} \right) \frac{\partial k}{\partial x_i} \right] + P_k + G - \rho \varepsilon \quad (5)$$

ε Equation

$$\frac{\partial(\rho \varepsilon)}{\partial t} + \frac{\partial(\rho \bar{\mathbf{u}}_i \varepsilon)}{\partial x_i} = \frac{\partial}{\partial x_i} \left[\left(\mu + \frac{\mu_t}{\sigma_\varepsilon} \right) \frac{\partial \varepsilon}{\partial x_i} \right] + C_1 \frac{\varepsilon}{k} (P + C_3 G) - C_2 \rho \frac{\varepsilon^2}{k} \quad (6)$$

where the model constants are:

$$C_\mu = 0.09, C_1 = 1.44, C_2 = 1.92, C_3 = 1.0, \sigma_k = 1.0 \text{ and } \sigma_\varepsilon = 1.217$$

The $\rho \varepsilon$ term in Eq. (5) is the destruction rate, μ is the viscosity (kg/m s), P_k is the shear production [13] and G is the buoyancy production [13]:

$$P_k = \mu_t \frac{\partial \bar{\mathbf{u}}_i}{\partial x_j} \left(\frac{\partial \bar{\mathbf{u}}_i}{\partial x_j} + \frac{\partial \bar{\mathbf{u}}_j}{\partial x_i} \right) \quad (7)$$

$$G = g_i \beta \frac{\mu_t}{Pr} \left(\frac{\partial \bar{T}}{\partial x_i} \right) \quad (8)$$

where Pr is the Prandtl number. The eddy viscosity (μ_t , kg/m s) is defined from dimensional analysis as

$$\mu_t = \rho C_\mu \frac{k^2}{\varepsilon} \quad (9)$$

Mass Transfer in Air

In this study, the fluid in the empty rubber-sheet drying chamber is a mixture of air, which is the continuous phase, and the droplets of vapour, which is the dispersed phase. Both can be described by Fick's law of mass transfer [17]:

$$\frac{\partial(\rho Y)}{\partial t} + \nabla \cdot (\rho \bar{\mathbf{u}} Y) = -\nabla \cdot \bar{\mathbf{J}} + S \quad (10)$$

$$\bar{\mathbf{J}} = -\left(\rho D_m + \frac{\mu}{Sc} \right) \nabla Y \quad (11)$$

where $\bar{\mathbf{J}}$ is the diffusion flux (kg/m²s), Y is the mass fraction of water vapour in air (kg water/kg dry air), D_m is the diffusion coefficient of water vapour in air (m²/s), and Sc is the Schmidt number of turbulent flow.

CFD Programme

We performed 3D simulations using the ANSYS Fluent, version 13, CFD software. The finite volume method in the programme was used to calculate the temperature and relative humidity distributions in the model chamber. The force convective terms were discretised using a first-order upwind scheme [13]. The pressure-velocity coupling was solved using the SIMPLE discretisation algorithm [13].

COMPARISON

The temperature and relative humidity in the model chamber using the single-phase and multiphase models were derived and compared with the experimental results to assess the agreement.

Experiments

The drying chamber dimensions are $1.2\text{ m} \times 1.2\text{ m} \times 1.2\text{ m}$, as shown in Figure 1. The inlet air was heated by eight electrical heater sets (6 x 600W and 2 x 2kW). Temperatures at 32 positions, as shown in Figure 2, were measured by type-K thermocouples. The air relative humidity was measured using a probe (Rense, HT-740-T-1) at the location shown in Figure 2. A hot wire-type anemometer (Testo, 405-V1) was used to measure the air velocity at three points at the inlet of the chamber. The average value was used as the boundary condition at the inlet in the simulation. All data were continuously recorded using a data logger (Data-Taker, DT 605) at 1 min. intervals.

We investigated the temperature and relative humidity distribution in the drying chamber. The results, as shown in Figure 3, show that the temperature in each plane in the drying chamber increased rapidly during the initial stage and then gradually until a steady state was attained. The largest average temperature difference between any planes is 4° . The relative humidity, as anticipated, decreased with increasing temperature, as shown in Figure 4. The initial and final relative humidity values are 61.1% and 28% respectively.

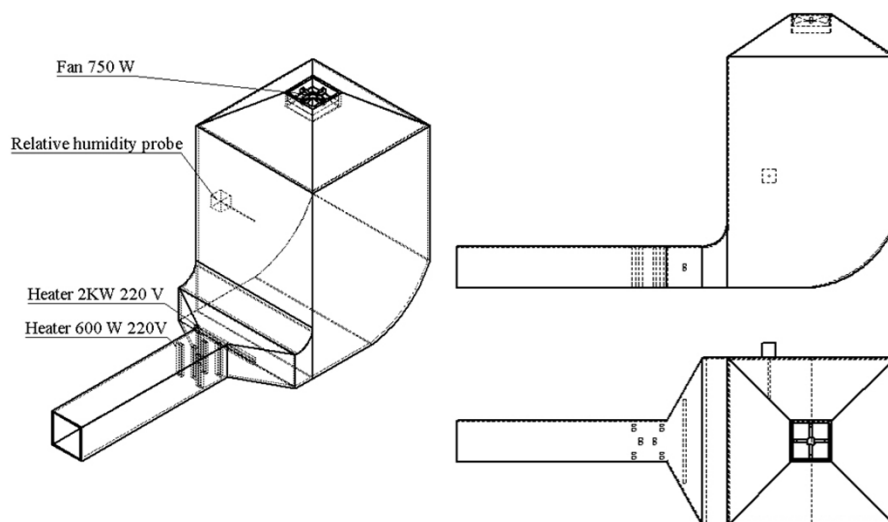


Figure 1. Schematic of the model rubber-sheet drying chamber

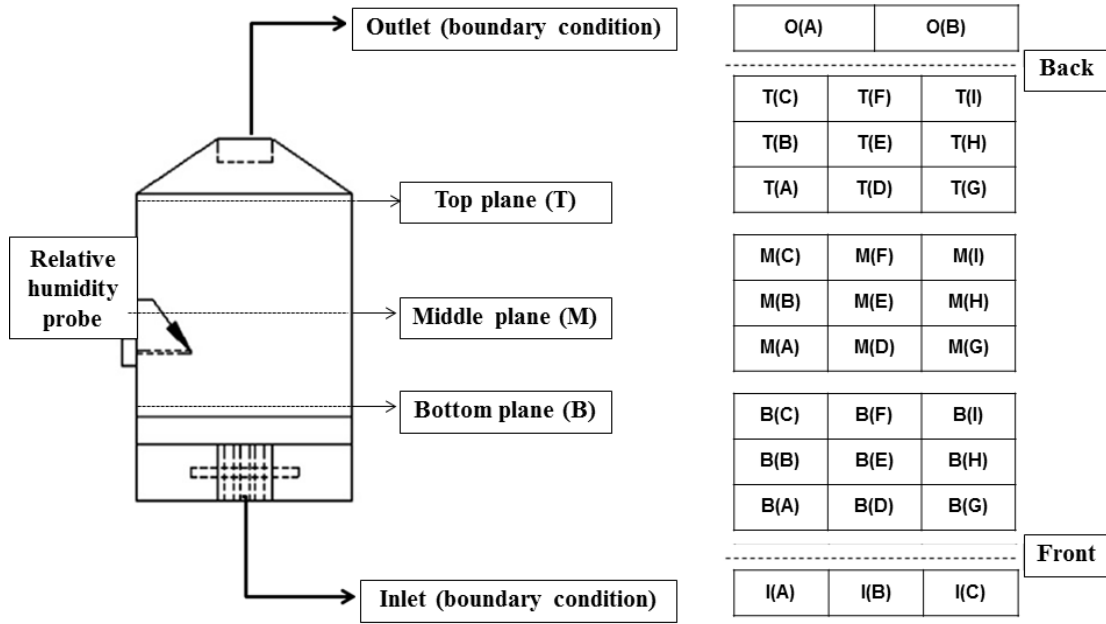


Figure 2. Positions of temperature and relative humidity probes in each plane

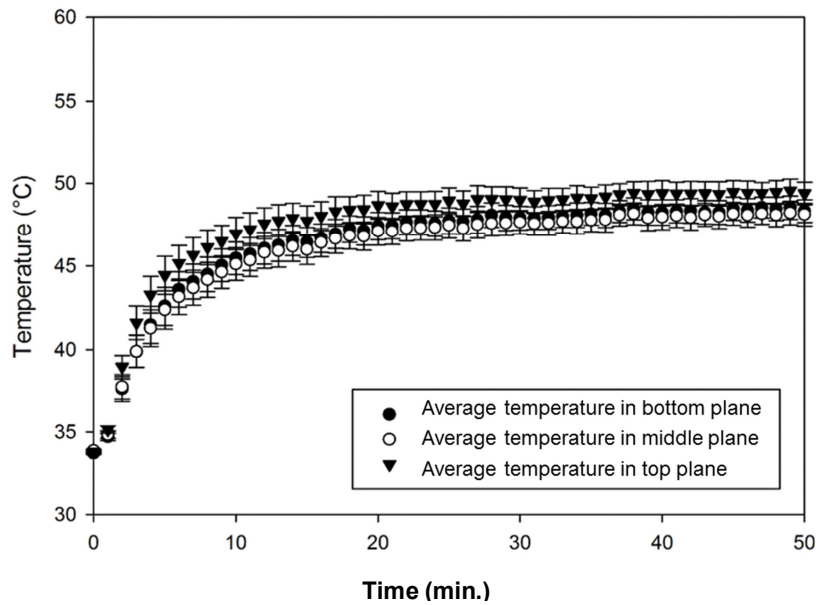


Figure 3. Average temperature as a function of time in the model drying chamber

Simulation

The model flow is fully symmetrical along the central plane of the chamber. The symmetrical condition is considered in the simulation to minimise the discrepancies when using the 3D half-size chamber in Figure 5. To minimise the computational time and avoid nonconvergence, we used the 3D half-size model in the simulations. The element-type tetrahedral and patch conformation algorithms were used to set the grid cells. The initial and boundary conditions in the simulations are described in the next section. Simulations were performed until steady state was reached; that is, after about 50 min.

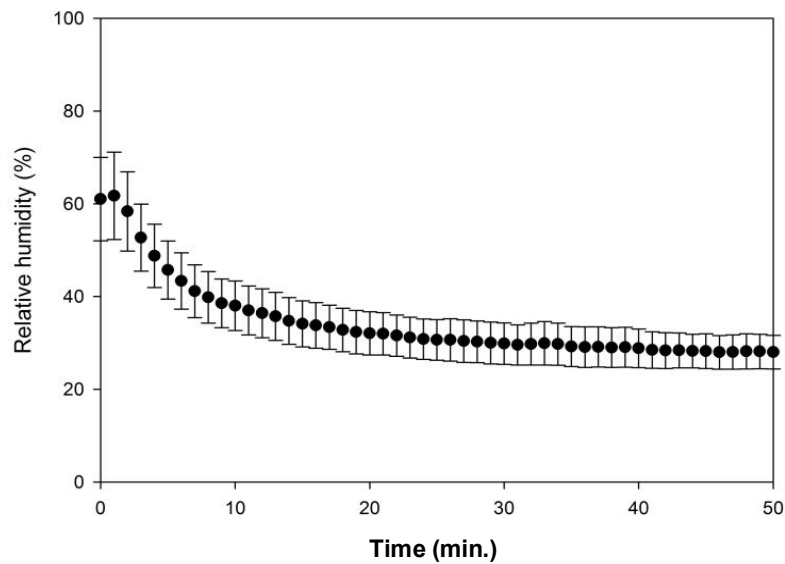


Figure 4. Relative humidity as a function of time in the model drying chamber

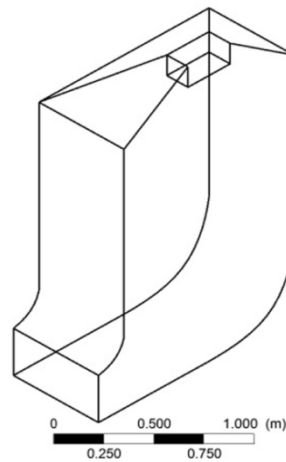


Figure 5. 3D half-size chamber used in the simulations

Initial and Boundary Conditions

Initial conditions

The initial temperature obtained from the experiments was 30.2°. The initial volume fraction of water vapour in air was 0.030416 (m³ of water vapour/m³ of dry air). This value was calculated from the measured relative humidity of 60% and the dry-bulb temperature of 33.0°. Thus,

$$v = w_s \left[\frac{\rho_{dry-air}}{\rho_{water-vapour}} \right] \quad (12)$$

where v is the volume fraction of water vapour, w_s is the humidity ratio (kg_{water vapour}/kg_{dry air}), $\rho_{water-vapour}$ is the density of water vapour, and $\rho_{dry-air}$ is the density of dry air.

Boundary conditions

At the inlet, the experimental constant inlet air velocity was 0.725 m/s. The user-defined function of the inlet temperature and vapour volume fraction were used as boundary conditions.

At the outlet, the pressure was set at zero. The experimental outlet temperature data as a function of time were fitted and used as boundary conditions in the user-defined function. At the wall, experimental heat flux data as a function of time were fitted and used as boundary conditions in the user-defined function.

Computational Validation

A grid sensitivity test was performed using three different mesh schemes, as shown in Table 1. For the bottom-plane temperature, the comparison between the simulation and experiments is shown in Figure 6. The simulation results using the coarse grid are not sufficiently accurate when compared with the experimental results. The simulation results using the medium and fine grids agree well with the experimental results. Discrepancies of 0.01-1.05% are seen using the medium grid, which is deemed satisfactory compared with the fine grid scheme. Therefore, the minimal grid refinement of 83,649 was used in the simulation.

Table 1. Grid schemes used in the convergence test

| | Case 1 (coarse) | Case 2 (medium) | Case 3 (fine) |
|---------|-----------------|-----------------|---------------|
| Node | 9,530 | 17,397 | 32,695 |
| Element | 59,469 | 83,649 | 163,601 |

RESULTS AND DISCUSSION

Temperature

Single-phase models have been rigorously evaluated by other researchers; hence we concentrated on the multiphase model. Nevertheless, we also compared the temperature predictions of the single-phase and multiphase models.

Multiphase model vs experiment

The multiphase model temperature distribution in the bottom, middle and top planes, initially and after 50 min. at steady state, is shown in Figure 7. The initial and steady state temperature is respectively 33.85° and 49.64°. The temperature distribution in any plane is uniform with no significant differences between planes. The temperature deviations between experiments and simulations are 0.01-4.73° for the bottom plane, 0.02-4.05° for the middle plane, and 0.01-3.84° for the top plane, as shown respectively in Figures 8-10. The largest deviation of 4.73° occurs at the centre-frontal position of the bottom plane, which is denoted as B(D) in Figure 2, and is attributed to the proximity of the hot-gas inlet where the temperature is highly variable. However, the boundary temperature conditions in the simulations are constant. The centre-frontal position in the middle plane, denoted as M(D), is still affected by the hot gas from the inlet, as shown in Figure 9. The hot-gas effect decreases in the top plane where the temperature is rather uniform throughout, as shown in Figure 10. The comparison of the experimental and model temperatures shows acceptable agreement; thus, we can use the multiphase model to simulate the temperature distribution in the drying chamber.

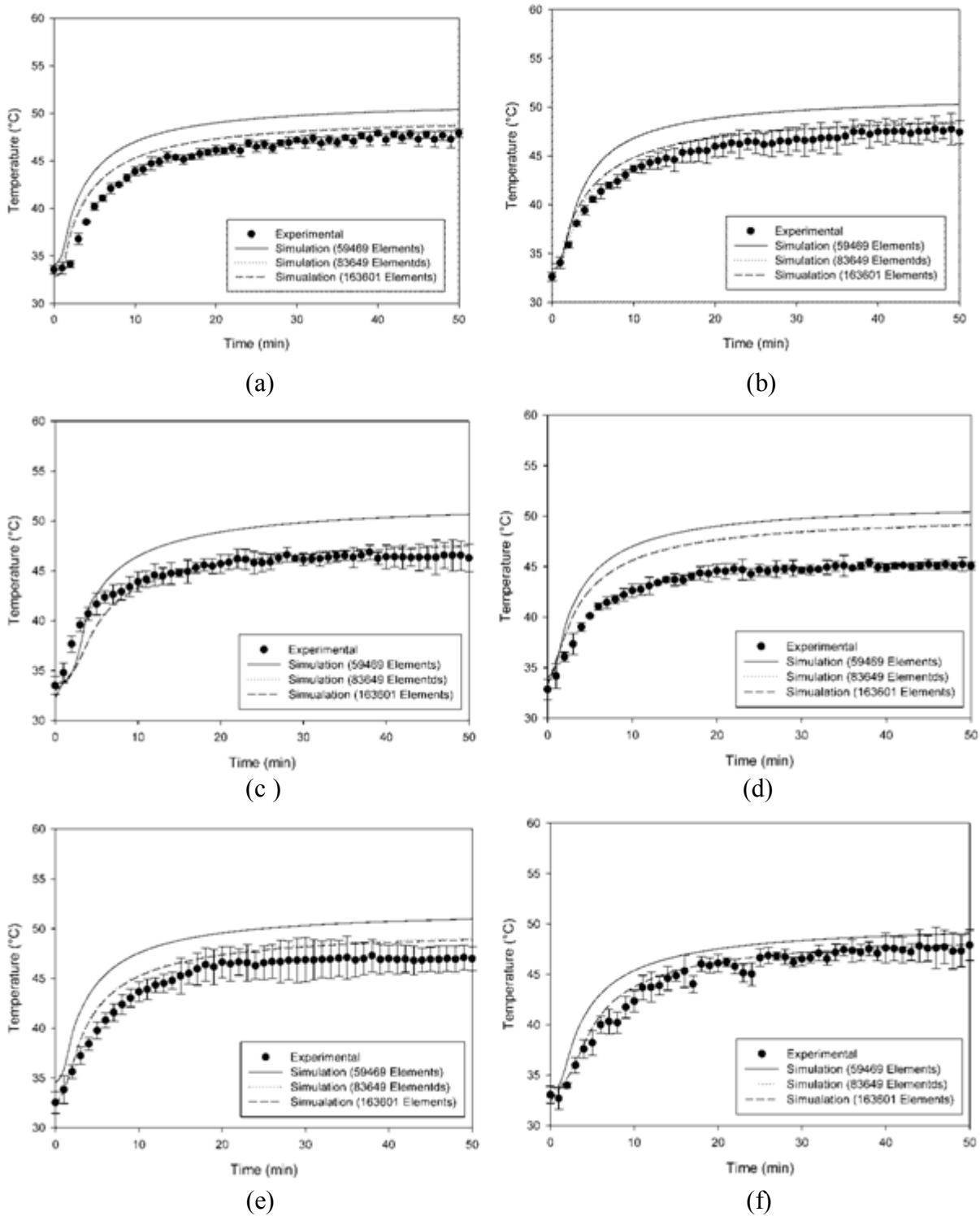


Figure 6. Plots of temperature as a function of time for experimental and simulation data for the multiphase model using the coarse (59,469 elements), medium (83,649 elements) and fine (163,601 elements) grid schemes in the bottom plane: (a) position B(A); (b) position B(B); (c) position B(C); (d) position B(D); (e) position B(E); (f) position B(F)

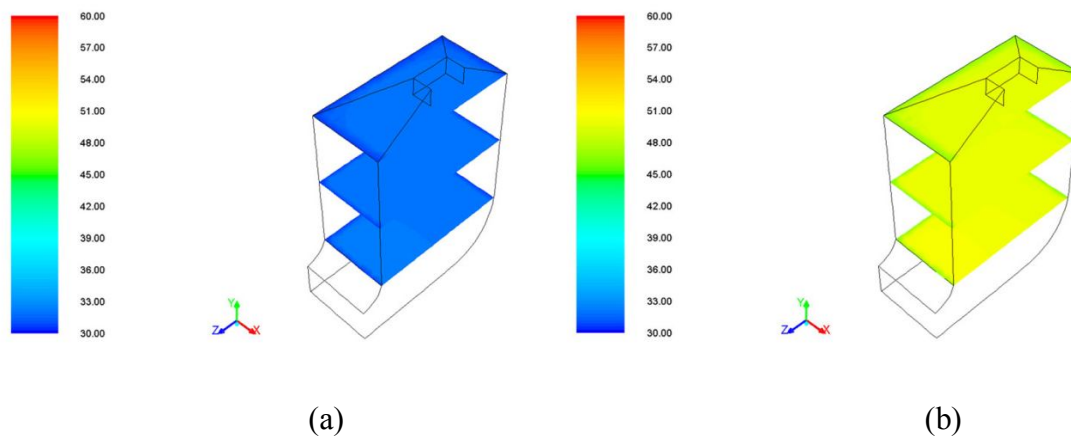


Figure 7. Temperature profile of bottom, middle and top planes in the model chamber at 0 min. (a) and 50 min. (steady state) (b)

Multiphase model vs single-phase model

The single-phase and multiphase model temperatures were compared with the experimental data for the largest deviation scenario (at the centre-frontal positions of all planes) and the smallest deviation scenario (at B(F), centre-back position of the bottom plane) and shown in Figures 11-13. The deviations at B(D) are $1.66-6.63^\circ$ and $0.51-4.73^\circ$ for the single-phase model and the multiphase model respectively. At B(F), the deviations for the multiphase model are minimal at $0.01-2.47^\circ$, whereas those of the single-phase model are $0.96-6.27^\circ$. Similar results are obtained in the middle and top plane, as shown in Figures 12 and 13 respectively. Initially, the multiphase model shows better agreement in the middle plane while the differences in the top plane are not clear. Overall, the multiphase model outperforms the single-phase model. The inclusion of humidity in the multiphase model decreases the air temperature compared with the single-phase model.

Relative Humidity

The relative humidity (RH) predicted by the multiphase model is shown in Figures 14 and 15. The RH distribution in the bottom, middle and top planes at the beginning and after 50 min. at steady state are shown in Figures 14 (a) and 14 (b) respectively. In all planes, the RH values are mostly uniform except near the centre-frontal area of the bottom plane. The largest deviation is initially seen with higher RH variation in the bottom plane, as shown in Figure 14. Apparently, the flow turbulence at the inlet induces variations in the moisture distribution. Moreover, the RH difference between minimum and maximum is initially much higher than that at steady state. The experimental and multiphase model data are compared in Figure 15. The deviations range between 0.56-10.45%, suggesting acceptable agreement and the suitability of the multiphase model.

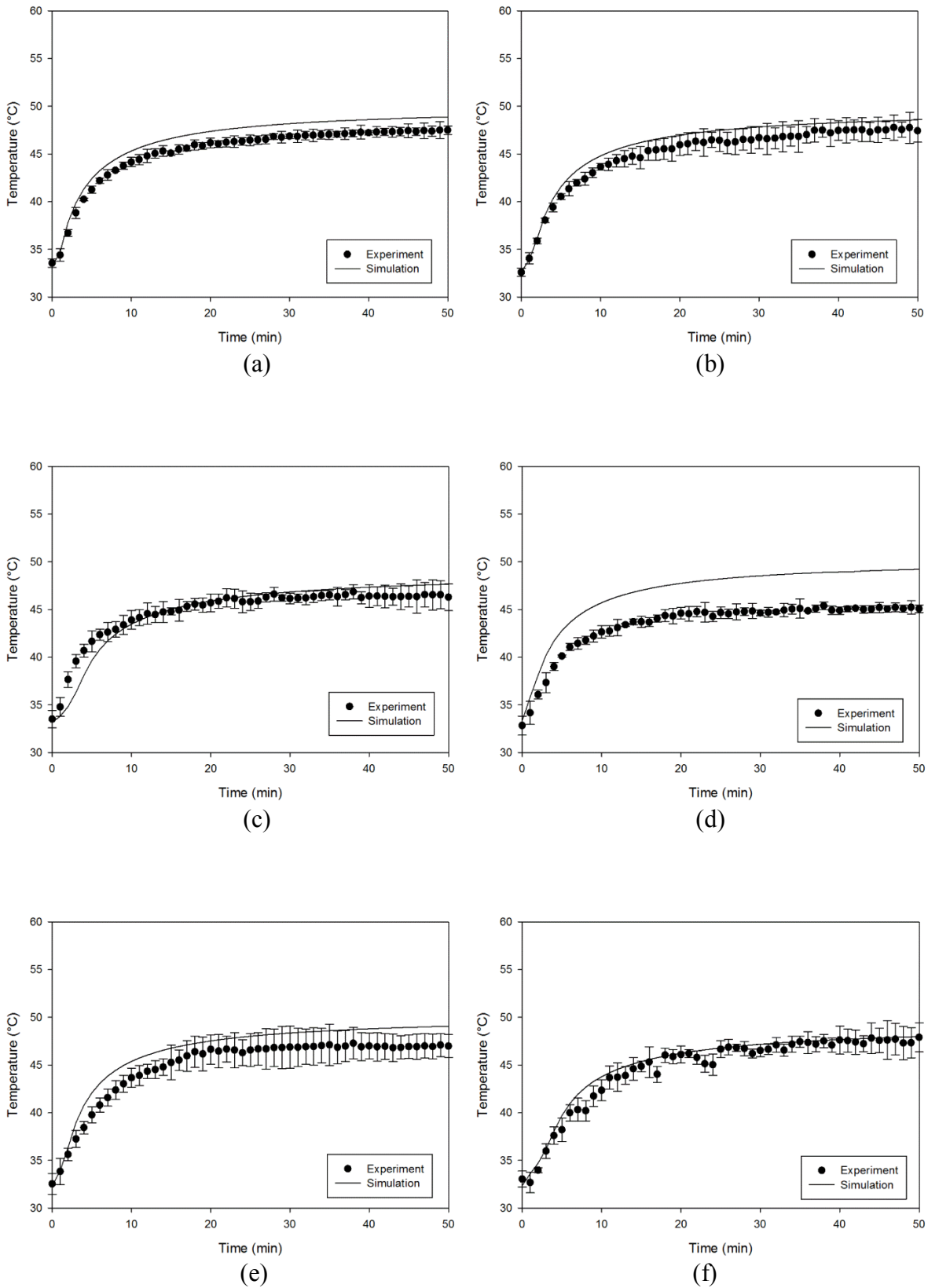


Figure 8. Plots of temperature as a function of time for the experiment and multiphase model in the bottom plane: (a) position B(A); (b) position B(B); (c) position B(C); (d) position B(D); (e) position B(E); (f) position B(F)

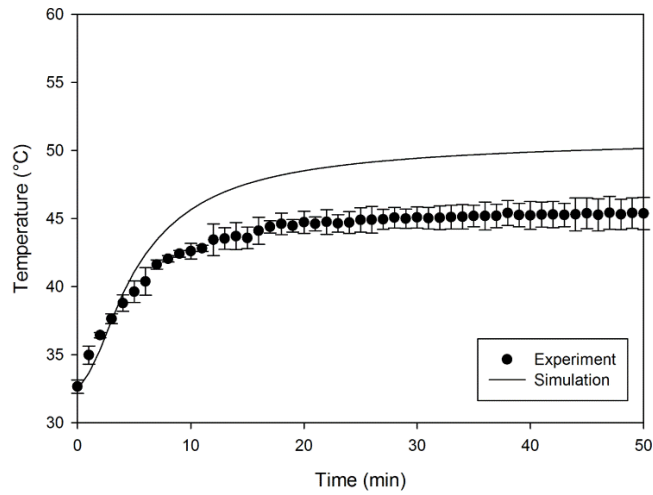


Figure 9. Plots of temperature as a function of time for the experiment and multiphase model in the middle plane (position M(D))

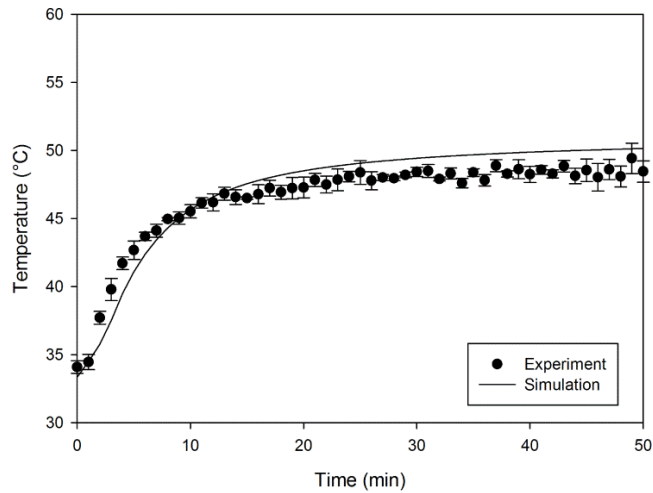


Figure 10. Plots of temperature as a function of time for the experiment and multiphase model in the top plane (position T(D))

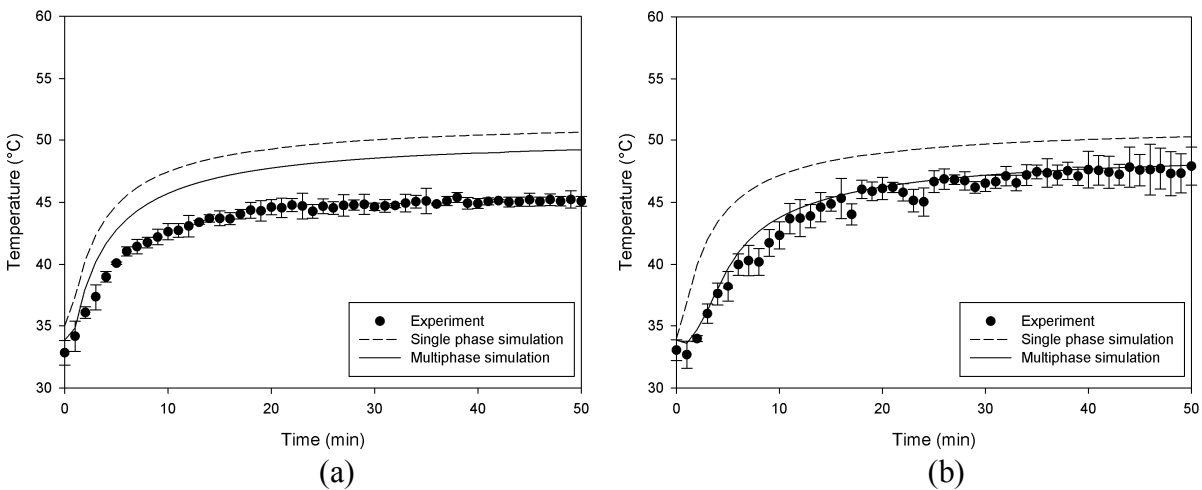


Figure 11. Plots of temperature as a function of time for the experiment and simulations in the bottom plane: (a) position B(D); (b) position B(F)

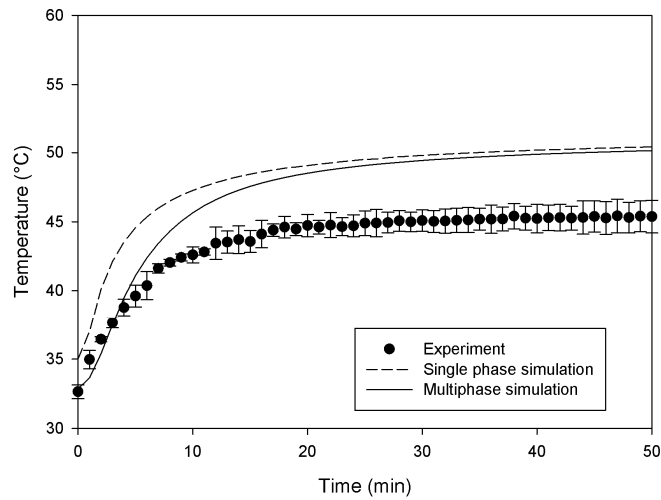


Figure 12. Plots of temperature as a function of time for the experiment and simulations in the middle plane (position M(D))

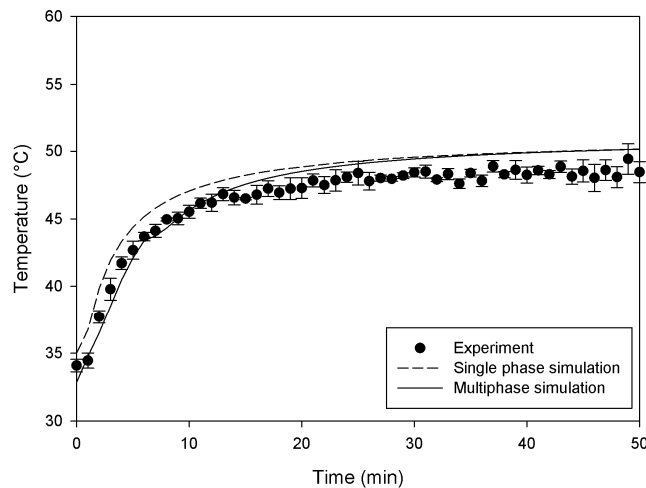


Figure 13. Plots of temperature as a function of time for the experiment and simulations in the top plane (position T(D))

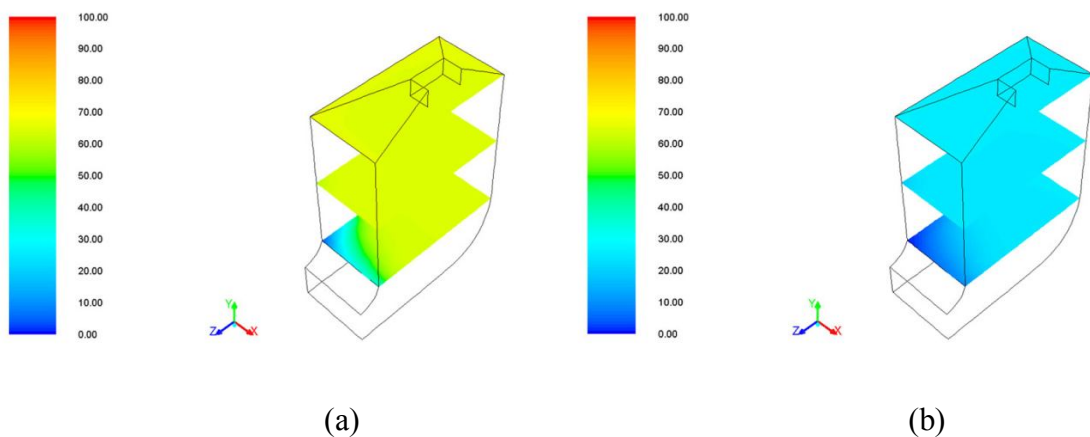


Figure 14. Relative humidity (%) profile of the bottom, middle and top planes in the drying chamber at 0 min. (a) and 50 min. (steady state) (b)

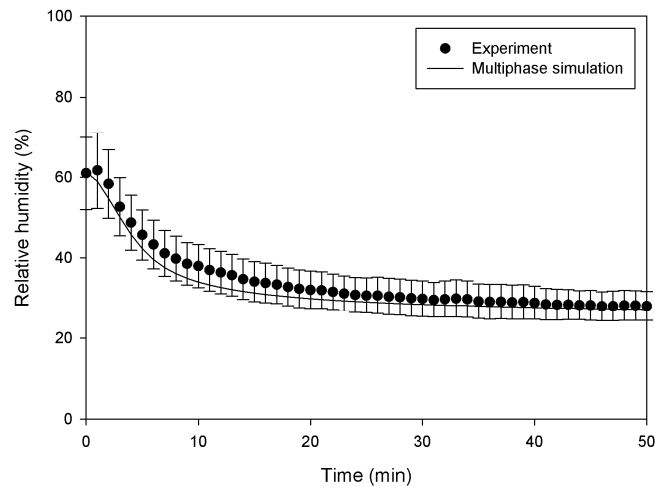


Figure 15. Plots of relative humidity as a function of time in the drying chamber

CONCLUSIONS

Temperature and relative humidity distributions in a model rubber-sheet drying chamber were simulated using CFD. For temperature, the multiphase model is superior to the single-phase model. The largest temperature deviation is seen at the centre-frontal location owing to the turbulence of the hot gas at the inlet. As for relative humidity, the multiphase model well reproduces the experimental results. The multiphase model can thus be used to simulate and reliably predict the temperature and relative humidity distribution in a chamber containing rubber sheets. Nonetheless, the diffusion of moisture from the sheets has to be included in the simulation to obtain the optimal conditions for energy savings.

ACKNOWLEDGEMENTS

This study was supported by the Higher Education Research Promotion and National Research University Project of Thailand, Office of the Higher Education Commission. We also thank Mr. Wiwat Sutiwipakorn for editing the manuscript.

REFERENCES

1. C. Y. Wang and P. Cheng, "A multiphase mixture model for multiphase, multicomponent transport in capillary porous media—I. Model development", *Int. J. Heat Mass Transf.*, **1996**, *39*, 3607-3618.
2. V. Mathiesen, T. Solberg and B. H. Hjertager, "An experimental and computational study of multiphase flow behavior in a circulating fluidized bed", *Int. J. Multiphase Flow*, **2000**, *26*, 387-419.
3. P. Spicka, M. M. Dias and J. C. B. Lopes, "Gas-liquid flow in a 2D column: Comparison between experimental data and CFD modelling", *Chem. Eng. Sci.*, **2001**, *56*, 6367-6383.
4. S. Venkateswaran, J. W. Lindau, R. F. Kunz and C. L. Merkle, "Computation of multiphase mixture flows with compressibility effects", *J. Comput. Phys.*, **2002**, *180*, 54-77.
5. M. V. Tabib, G. Lane, W. Yang and M. P. Schwarz, "CFD study of single phase and multiphase (liquid-liquid) pump-mixer: Analyzing design parameters, flow structures and turbulence", *Chem. Eng. Sci.*, **2012**, *80*, 55-69.

6. B. Xia and D. W. Sun, “Applications of computational fluid dynamics (CFD) in the food industry: A review”, *Comput. Electron. Agric.*, **2002**, 34, 5-24.
7. P.-S. Mirade, “Prediction of the air velocity field in modern meat dryers using unsteady computational fluid dynamics (CFD) models”, *J. Food Eng.*, **2003**, 60, 41-48.
8. E. Mathioulakis, V. T. Karathanos and V. G. Belessiotis, “Simulation of air movement in a dryer by computational fluid dynamics: Application for the drying of fruits”, *J. Food Eng.*, **1998**, 36, 183-200.
9. J. Smolka, A. J. Nowak and D. Rybarz, “Improved 3-D temperature uniformity in a laboratory drying oven based on experimentally validated CFD computations”, *J. Food Eng.*, **2010**, 97, 373-383.
10. J. Cui and S. Wang, “Application of CFD in evaluation and energy-efficient design of air curtains for horizontal refrigerated display cases”, *Int. J. Therm. Sci.*, **2004**, 43, 993-1002.
11. P.-S. Mirade, A. Kondjoyan and J.-D. Daudin, “Three-dimensional CFD calculations for designing large food chillers”, *Comput. Electron. Agric.*, **2002**, 34, 67-88.
12. T. A. G. Langrish and D. F. Fletcher, “Spray drying of food ingredients and applications of CFD in spray drying”, *Chem. Eng. Process.*, **2001**, 40, 345-354.
13. M. Promtong and P. Tekasakul, “CFD study of flow in natural rubber smoking-room: I. Validation with the present smoking-room”, *Appl. Thermal Eng.*, **2007**, 27, 2113-2121.
14. P. Tekasakul and M. Promtong, “Energy efficiency enhancement of natural rubber smoking process by flow improvement using a CFD technique”, *Appl. Energ.*, **2008**, 85, 878-895.
15. H. K. Versteeg and W. Malasekera, “An Introduction to Computational Fluid Dynamics: The Finite Volume Method”, Pearson Education, Essex, **1995**.
16. J. D. Anderson, “Computational Fluid Dynamics: The Basics with Applications”, McGraw-Hill, New York, **1995**.
17. R. B. Bird, W. E. Stewart and E. N. Lightfoot, “Transport Phenomena”, 2nd Edn., John Wiley and Sons, New York, **2007**.